Aerodynamic design optimization of nacelle/pylon position on an aircraft

Li Jing, Gao Zhenghong *, Huang Jiangtao, Zhao Ke

National Key Laboratory of Aerodynamic Design and Research, Northwestern Polytechnical University, Xi'an 710072, China

Abstract   The arbitrary space-shape free form deformation (FFD) method developed in this paper is based on non-uniform rational B-splines (NURBS) basis function and used for the integral parameterization of nacelle-pylon geometry. The multi-block structured grid deformation technique is established by Delaunay graph mapping method. The optimization objects of aerodynamic characteristics are evaluated by solving Navier–Stokes equations on the basis of multi-block structured grid. The advanced particle swarm optimization (PSO) is utilized as search algorithm, which combines the Kriging model as surrogate model during optimization. The optimization system is used for optimizing the nacelle location of DLR-F6 wing-body-pylon-nacelle. The results indicate that the aerodynamic interference between the parts is significantly reduced. The optimization design system established in this paper has extensive applications and engineering value.

© 2013 Production and hosting by Elsevier Ltd. on behalf of CSAA & BUAA.
Open access under CC BY-NC-ND license.

1. Introduction

At present the layout of wing-mounted engine is generally used at the large transport aircraft. This kind of layout has numerous merits, but large interference drag is probably caused between the wing/pylon/nacelle and the aerodynamic performance is affected accordingly. For a long time, a great deal of effort has been made on the aerodynamic disturbance between the wing/pylon/nacelle by the aircraft design engineers. As early as in the 1980s, Refs.[1–3] presented the PAN AIR method which was coupled to three-dimensional boundary layer analysis for aerodynamic analysis and design of the wing/nacelle configuration, and the interference drag between wing and nacelle was reduced. Based on full potential equation, Saitoh et al.[4] applied the multi-disciplinary optimized methods to carry out the optimization of the nacelle position. Gisin and Marshall[5] had developed the optimization design of the inboard wing/nacelle position using the superficial grid migration method. Moreover, there are many other elaborations about wing/body/pylon/nacelle design method.[6–9] Since the integrated distortion of pylon and nacelle is very difficult to be realized, and the grids automatic divisions are difficult as well, the optimization of the nacelle position is carried on the non-pylon situation at present, or the other design method is "cut and try" which is generally used in the engineering application. However, these methods are difficult to satisfy the modern aircraft design requirements. Firstly, the disturbance between pylon and nacelle/wing does physically exist, and the drag of pylon changes with the nacelle position. All

* Corresponding author. Tel.: +86 029 88492906.
  E-mail addresses: jingself@163.com (J. Li), zgao@nwpu.edu.cn
(Z. Gao).

the mentioned issues may cause certain deviation on nacelle position optimization result when the pylon is installed. Secondly, when the coupling influence between nacelle and pylon is considered into the design process, the massive manpower and the physical resource will be thrown in "cut and try", while it is difficult to obtain a best design result. For example, when the better performance engine was changed for Boeing 737-300 based on the prototype aircraft, the interference drag was increased by the larger nacelle. The partial wing shape, nacelle shape and installation position were adjusted by the design engineers again and again, while the massive numerical simulation was carried out.[1]

To build an optimal design system which is used for the wing-pylon-nacelle optimization, there are three key techniques to be resolved: (A) an efficient and robust geometry modification method is required especially for juncture regions, and the fast/robust grid distortion technology becomes important concerns; (B) for new design variables, the key which directly affect the design result and efficiency is whether the aerodynamic characteristics of the corresponding geometry can be obtained fast and exactly; (C) the optimized algorithm used in the process dominates the optimization efficiency for aerodynamic optimization design as well as the overall convergence.

In connection with the optimization design requirements of the modern transport, the wing-body-pylon-nacelle optimization design system has been developed in this study based on the arbitrary space free form deformation (FFD) technology,[10,11] and the dynamic spatial grid distortion technology[12–16] for the multi-block structured grid is developed for complex aircraft configurations such as wing-body- pylon-nacelle. The present design system is applied to DLR-F6 wing-body-pylon-nacelle configuration. This configuration has strong aerodynamic interference at cruise condition. The design objective is to reduce the interference drag.

2. Complex shape parameterization method and spatial grids distortion technology

2.1. Arbitrary space FFD parameterization technique

Arbitrary shape framework and control vertices can be built for arbitrary spaces. By embedding the object which is consistent with the FFD space into this framework and manipulating control points of the lattice, the deformation of the object with better flexibility can be achieved. Following the above steps, we can derive arbitrary deformation of the object by controlling points.[10,11] This method is different from the traditional FFD. The traditional FFD parameterizes initial geometry and the shape perturbations are added to the initial geometry.

Arbitrary space FFD technique is built in this paper, which can maintain the continuity of arbitrary order derivative for deformed object.[17] Non-uniform rational B-spline (NURBS) basic function is constructed as spatial attributes, so the mapping function $X = F(x)$ from Cartesian space to the parameter space $R^3 \rightarrow R'^3$ can be set up. The Cartesian coordinate of an arbitrary point X in the framework can be expressed as

$$X(s,t,u) = \sum_{i=0}^{l}\sum_{j=0}^{m}\sum_{k=0}^{n} P_{i,j,k} B_{il}(s) B_{jm}(t) B_{kn}(u) \tag{1}$$

where $B_{il}(s)$, $B_{jm}(t)$ and $B_{kn}(u)$ are respectively NURBS basic functions of l, m, n order, and $P_{i,j,k}$ represents the control vertices. When the reciprocity between the object and framework is established, we can obtain a new control vertex $P'_{i,j,k}$ and the deformed control framework by changing the displacement of control vertex $P_{i,j,k}$ in control volume. If the local coordinate of any point X in original control volume is (s, t, u), the corresponding Cartesian coordinates X_{FFD} after deformation of the framework at that point can be calculated by:

$$X_{FFD} = \sum_{i=0}^{l}\sum_{j=0}^{m}\sum_{k=0}^{n} P'_{i,j,k} B_{il}(s) B_{jm}(t) B_{kn}(u) \tag{2}$$

Eq. (1) indicates that when the deformed object coordinates is calculated by the new control vertex, the local coordinates of any point X in original control volume (s, t, u) should be determined firstly. Generally, the nonlinear equations should be calculated according to the original control vertex and Eq. (1) in this process. For the local deformation, the framework and object intersect. So the location of the control points of the framework should be required strictly to maintain the continuity of cut vector and curvature.

For constructing more complex configuration framework, more FFD spaces are required. A continuous control of boundary conditions is established in this paper, which can be used to maintain the continuity of derivative vector. The continuity of derivative vector conditions can be expressed as

$$\begin{cases} \dfrac{\partial X_{1FFD}(0,t_1,u_1)}{\partial s_1} = \dfrac{\partial X_{2FFD}(0,t_2,u_2)}{\partial s_2} \\[2mm] \dfrac{\partial X_{1FFD}(0,t_1,u_1)}{\partial t_1} = \dfrac{\partial X_{2FFD}(0,t_2,u_2)}{\partial t_2} \\[2mm] \dfrac{\partial X_{1FFD}(0,t_1,u_1)}{\partial u_1} = \dfrac{\partial X_{2FFD}(0,t_2,u_2)}{\partial u_2} \end{cases} \tag{3}$$

In this paper, FFD space deformation technique in the form of multi-zone, separation/patched is applied to DLR-F6 wing-body-pylon-nacelle complex shape parameterization. The control framework is divided into two regions. The transformation is respectively carried on from Cartesian coordinate to logical coordinate, as well as logical coordinate to Cartesian coordinate in the region. 12 FFD control vertexes are shared between the two regions. To maintain the continuity of pylon and nacelle, the displacement of these shared vertexes should be consistent. Fig. 1 shows the control framework and control vertexes. The deformation of pylon is controlled by the upper framework, and the rigid migration of the nacelle is controlled by the lower framework as well. The description of installed parameters can be realized by the rigid translation and
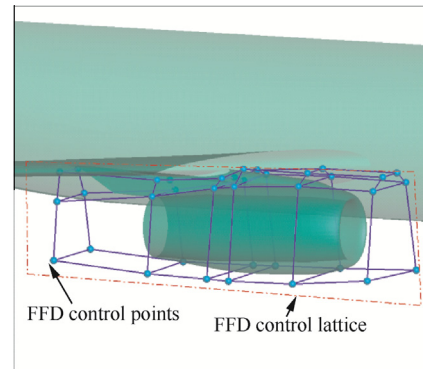

Fig. 1 FFD control framework and vertexes.

(a) Vertical movement
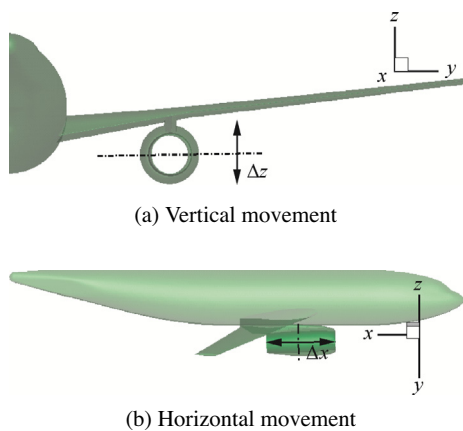

(b) Horizontal movement

Fig. 2   Nacelle design variable.

rotation of the lower framework. In this paper, some installed parameters have been given, and the vertical movement and horizontal movement are realized through the rigid migration of the lower framework. Fig. 2 show the vertical movement and horizontal movement which are considered as design variables in this study.

The optimization of the pylon is not carried out in this paper. The pylon will be deformed smoothly as the change of the nacelle's position. The rigid migration of the nacelle is controlled by the 12 control vertexes of the lower framework. The displacement of the 12 control vertexes must be the same because the shape of the nacelle keeps unchanging. Therefore there are two design variables in this paper. One is the streamwise position, and the other is the height of the nacelle.

2.2. Delaunay graph mapping grid deformation technique

Transfinite interpolation (TFI) and elasticity deformation technique are used in structured grid deformation, but they are not suitable for large deformation cases. Delaunay graph mapping method is widely used in grid deformation domain for its robust and high efficiency. Given a set of boundary control points in computational plane or space, only one Delaunay triangulation can be achieved according to Delaunay algorithm.[12–16] Then the computational region will be covered with Delaunay triangle graph, and any grid points in computational region should be located in the triangulation. The algorithm introduced in reference[13] can be used to locate the triangulation where the grid points are.

For the plane Delaunay triangle grid, the mapping relation between calculated grid and plane Delaunay triangle grid is
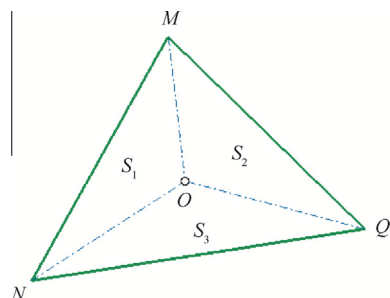

Fig. 3   Delaunay triangle and grid point.

established in Fig. 3.[16] According to the location of grid point and Delaunay triangle graph as shown in Fig. 3,[16] the areas of triangle MNQ, MON, NOQ and QOM are respectively S, S_1, S_2 and S_3. The weight coefficients ω_1, ω_2, ω_3 are expressed as

$$\begin{aligned} \omega_1 &= S_1/S \\ \omega_2 &= S_2/S \\ \omega_3 &= S_3/S \end{aligned} \tag{4}$$

Then the expression of relations would be established:

$$X_O = \begin{bmatrix} \omega_1 \\ \omega_2 \\ \omega_3 \end{bmatrix}^{\mathrm{T}} [X_M \ X_N \ X_Q] \tag{5}$$

where X_O is the grid point and $[X_M \ X_N \ X_Q]$ is the Delaunay triangle point.

With the update of the aerodynamic configuration finished, the Delaunay triangle graph will be deformed. For points $[X_M \ X_N \ X_Q]$ updated to the new location $[X'_M \ X'_N \ X'_Q]$, the grid points will be changed as

$$X'_O = \begin{bmatrix} \omega_1 \\ \omega_2 \\ \omega_3 \end{bmatrix}^{\mathrm{T}} [X'_M \ X'_N \ X'_Q] \tag{6}$$

The three-dimensional grid deformation method is coincident with two dimension case in principle. The weight coefficients ω_1, ω_2, ω_3 are defined by the volume of the tetrahedrons constructed by the grid points and Delaunay tetrahedron. The grid points and Delaunay tetrahedron are shown in Fig. 4,[16] the volume of tetrahedron $MNQP$, $MONP$, $QOMP$ and $MNOQ$ are respectively V, V_1, V_2 and V_3. The Delaunay tetrahedron section of the optimization example in this paper is shown in Fig. 5.
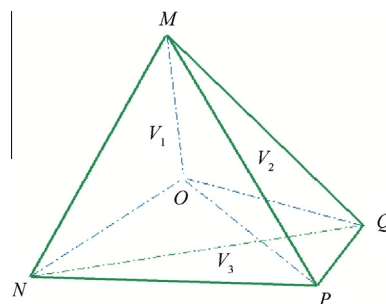

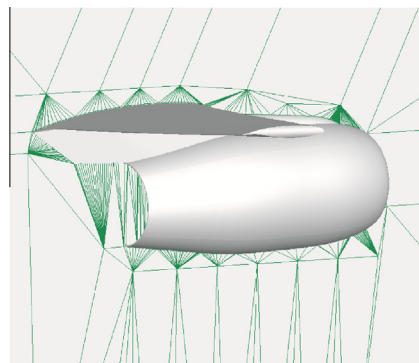**Fig. 4**   Delaunay tetrahedron and grid point.

Fig. 5   Delaunay tetrahedron section.

3. Aerodynamic optimization system

3.1. The CFD method

The aerodynamic characteristics in the optimization are evaluated by solving Navier–Stokes equations based on multi-block structured grid. In this paper, Roe's spatial scheme, Menter k–ω shear stress transport turbulence model, lower upper symmetric Gauss seidel (LU-SGS) implicit time marching method, multi-grid and parallel computing technique are adopted.

The reliability of CFD codes is verified through numerical simulation of DLR-F6 wing-body-pylon-nacelle standard model. The computation condition is $Ma_\infty = 0.75$, $Re = 3.0 \times 10^6$. The multi-block structured grids are adopted, the whole flow filed is divided into 525 regions, and the surface of configuration is divided into 150 regions.[18–21]

Fig. 6 shows the whole superficial grids; Fig. 7 shows the partial grids of wing-pylon-nacelle; Fig. 8 shows the lift-drag
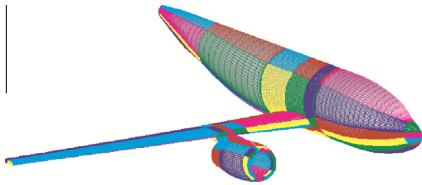

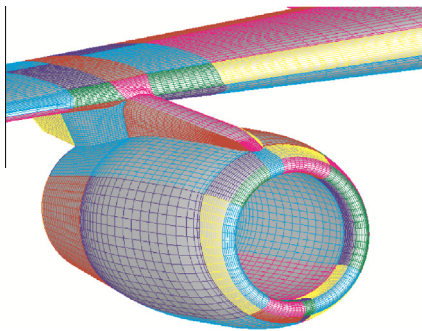**Fig. 6** The whole superficial grids of DLR-F6.

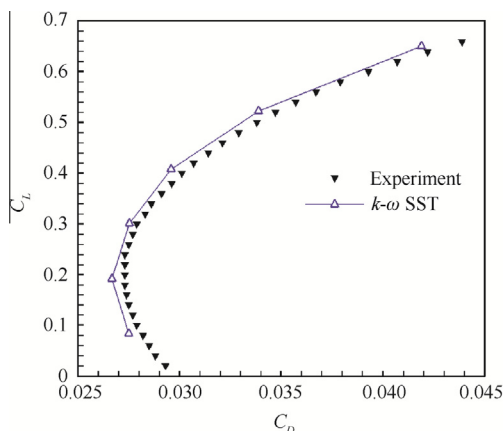**Fig. 7** Partial grids of wing-pylon-nacelle.
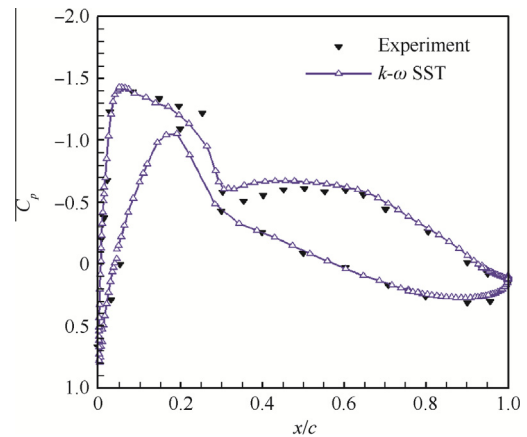

Fig. 8 Lift-drag polar curves.

Fig. 9 Wing pressure distributions of 33.1% span.

polar curve. The wing pressure distribution of 33.1% span is shown in Fig. 9. In this figures, C_L is the life coefficient, C_D is the drag coefficient, C_p is the pressure coefficient, and x/c is the span-chord ratio.

3.2. Experimental design and surrogate model

The common experimental design methods include completely randomized design, orthogonal design, uniform design, Latin hypercube design, etc. Latin Hypercube method is used here to select samples. The objects of samples are evaluated by the method which has been introduced in Section 3.1.

The application of surrogate model technology provides the possibility to large-scale optimization design, especially in CFD. The Kriging model,[22] which has good fitting results of multi-peak problems, is selected as the surrogate model of solving airfoil flow field problems in this paper.

The loose surrogate management framework is built up so as to improve the optimization efficiency.[23]

3.3. Optimization algorithm

By using the separated particle swarm optimization (PSO) method, one group is divided into several smaller sub-groups: the 1st sub-group, the 2nd sub-group, the 3rd sub-group and the 4th sub-group. Each of them evolves by various ways. Moreover, each sub-group has different searching assignment due to the unequal weight factor. The one having smaller weight factor searches in a local region, while the others having bigger weight factor will search globally. By this means, it can not only ensure the global optimization ability of the entire group, but also consider the local search ability. Suppose the 1st sub-group is defined as a local search region and the others are global search regions. The update on speed and location of each particle has the same formula as the standard particle swarm, which is given as

$$v_{i,j}(t+1) = \omega v_{i,j}(t) + c_1 r_1 (p_{i,j} - x_{i,j}(t))$$
$$+ c_2 r_2 (p_{g,j} - x_{i,j}(t))$$
$$x_{i,j}(t+1) = x_{i,j}(t) + v_{i,j}(t+1) \tag{7}$$

where ω is the weight factor, r_1 and r_2 are respectively the random numbers between 0 and 1, and c_1 and c_2 are learning factors, $v_{i,j}$ and $x_{i,j}$ are respectively the velocity and location of the
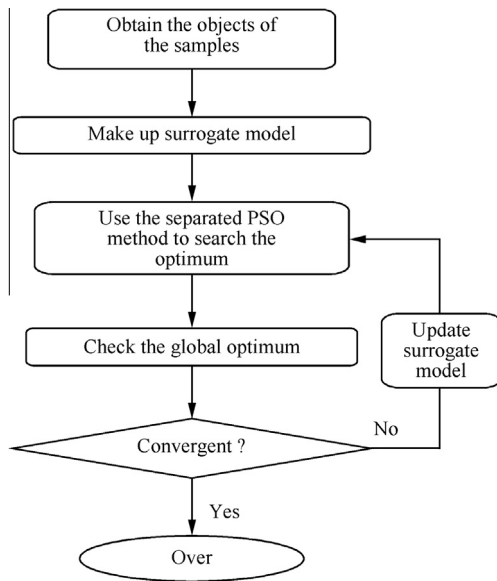
Fig. 10　Flowchart of design procedure.

particle swarm, $p_{i,j}$ and $p_{g,j}$ are respectively the personal best location and the global best location of the particle swarms.

For each sub-group, the selection of the global optimum location is different. The particle chose the global optimum location of the sub-group which it belongs to as its global optimum location. After the velocity and location of the particle updating, the global optimum location of each sub-group will update subsequently. Finally, the global optimum location of the 1st sub-group will be updated by those of other sub-groups,which can ensure the particle is always searching for the current optimum location when it is doing local search, and plays a positive role in accelerating convergence. The flowchart of the design procedure is shown in Fig. 10.

The function LevyNo.5 is chosen as the test function to verify the performance of optimization system. The function expression is as follows:

$$f(x) = \sum_{i=1}^{5}[i\cos((i-1)x_1+i)]\sum_{i=1}^{5}[j\cos((j+1)x_2+j)]$$
$$+ (x_1 + 1.42513)^2 + (x_2 + 0.80032)^2$$
$$- 10 \leqslant x_i \leqslant 10, \ i = 1, 2 \tag{8}$$

The LevyNo.5 function has a global minimum value -176.1375 at the point $(-1.3068, -1.4248)$. There are 760 local minimum value points in the domain of this function, so it is difficult to find the global minimum point. The convergent course is shown in Fig. 11. The finally optimal function value is -176.1370, and the optimal point is $(-1.3071, -1.4252)$.

4. Analysis of aerodynamic optimization

The position of nacelle has a very tremendous influence on the flow filed around the wing and the body. It may cause aerodynamic disturbance in various parts such as the wing, nacelle and pylon.[24,25] In this paper, with the consideration of the pylon deformed simultaneously, the interference drag of these parts would be reduced through optimizing the nacelle's vertical movement and horizontal movement.

The design cruise condition is as following: $Ma_\infty = 0.75$, $C_L = 0.50$, $Re = 3.0 \times 10^6$.

Based on design requirements, the following aerodynamic optimization mathematical model is established as follows:

(1) The object is min drag coefficient C_D.
(2) The constraint condition is $C_L = 0.50$.

In this optimization problem, 24 samples are produced by the Latin Hypercube method, and the object is evaluated for
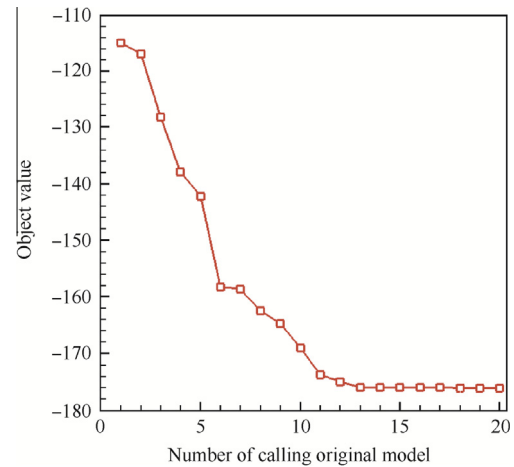

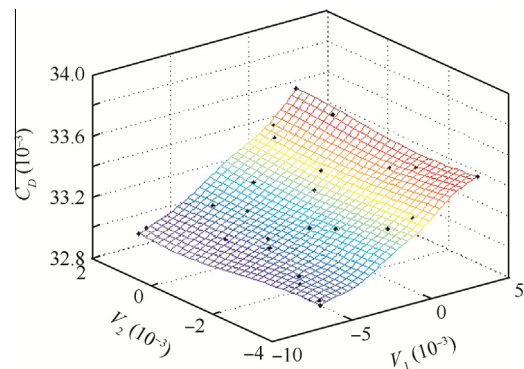**Fig. 11**　Optimization convergent course of test function.
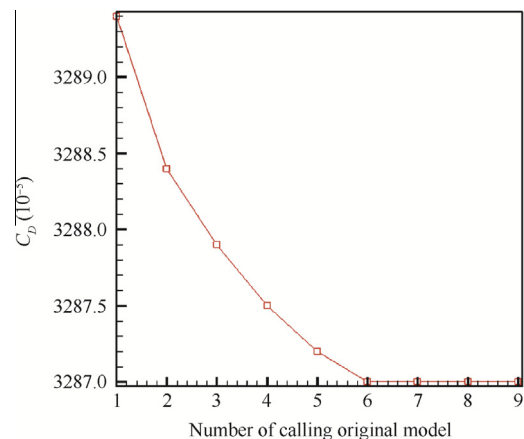

Fig. 12　Plot of initial response surface.

Fig. 13　Optimization convergent course.

each sample by the CFD method established in this paper, and then the surrogate model is built up. The initial response surface is shown in Fig. 12. The black points are the samples.

After every optimization process, the optimal particle is selected to check its object, and then to update the surrogate model. The optimization process will stop when the convergent condition is satisfied. The optimization convergent course is shown in Fig. 13.

The original position and optimized position of nacelle is shown in Fig. 14. Compared with the position of original con-

figuration, the optimized position is more forward and upward.

The wing pressure distribution of 34% span (on the inboard side of the pylon, approaching the pylon) of original configuration and optimized one is shown in Fig. 15. The optimization shows that the suction peak has been cut down and the strength of shock wave has been weakened. The cross section of pylon pressure distribution is shown in Fig. 16. The suction peak inboard of the pylon has been cut down; the local velocity and the pressure gradient have been reduced. The flow
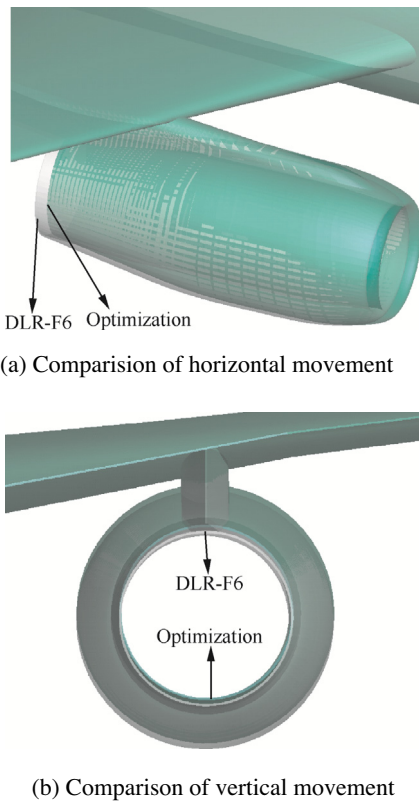

(a) Comparision of horizontal movement

(b) Comparison of vertical movement

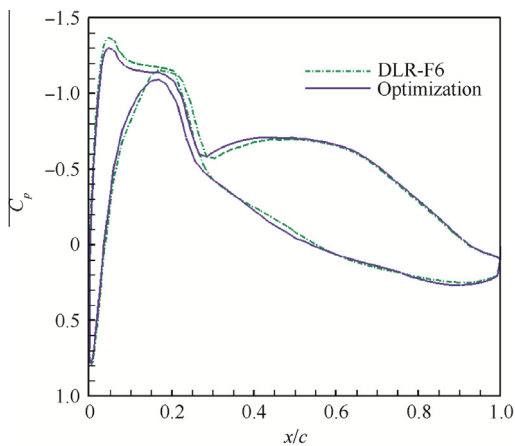**Fig. 14** Position comparison between the original configuration and optimized one.

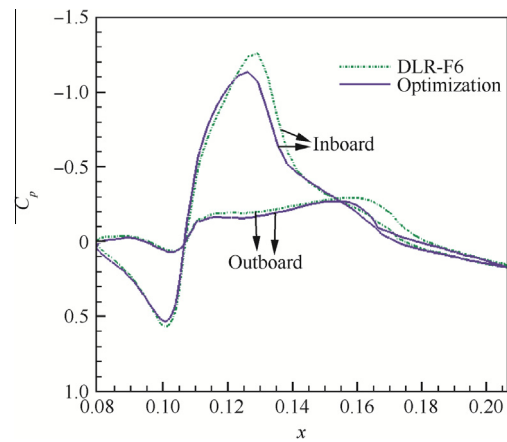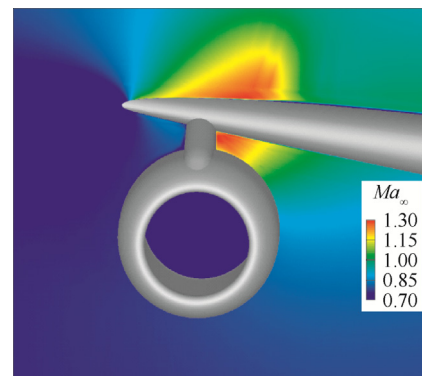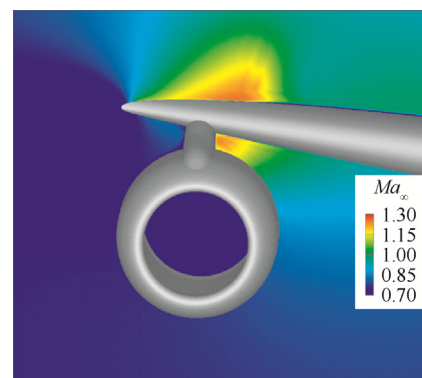**Fig. 15** Wing pressure distributions at 34% span.

Fig. 16 Pylon pressure distributions.

(a) Original configuration

(b) Optimized configuration

Fig. 17 Mach number contour of the flow field's cross section.

separation has been decreased, which results in smaller pressure drag.

Shock wave strength around pylon surface is remarkably reduced by the design. The Mach number contours of the flow field's cross section are shown in Fig. 17. The result of optimization shows that the local velocity of supersonic region located in the upper and lower wing has been reduced, and the aerodynamic interference has been weakened.

The superficial partial pressure contour of the original configuration and optimized one is shown in Fig. 18. The result of optimization shows that the local velocity inboard of the pylon has been reduced, the suction peak has been cut down, and then the strength of shock wave has been weakened. All the results of optimization show that the aerodynamic interference and the interference drag have been reduced. The comparison of aerodynamic characteristic between the original configuration and optimized one is shown in Table 1. The drag coefficient reduces 3.7 counts in the cruise condition.
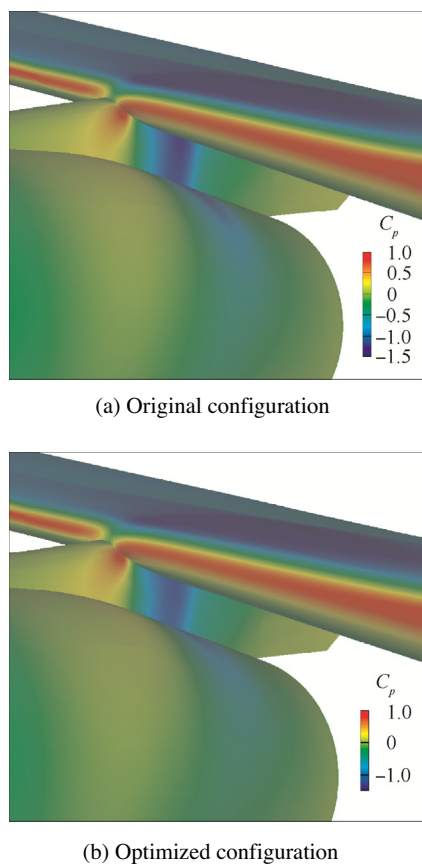

(a) Original configuration

(b) Optimized configuration

Fig. 18   Superficial partial pressure contour.

Table 1   Comparison of aerodynamic characteristic between the original configuration and optimized one.

State	C_L	C_D
Initial	0.5	0.03324
Optimization	0.5	0.03287

5. Conclusions

The optimization system for complex configuration has been set up in this paper. The arbitrary space-shape FFD method based on NURBS basis function is utilized as the aerodynamic shape parameterization method. The Delaunay graph mapping method is used for mesh deformation. The separated PSO method is taken as the optimization framework, and the Kriging model is introduced to the optimization process. The aerodynamic optimization design system is applied to DLR-F6 wing-body-pylon-nacelle. The results of optimization indicate that the complex configuration can be deformed simultaneously through the arbitrary space-shape FFD technique. The successful design results validate the effectiveness and efficiency of the present optimization design system established in this paper. Shock wave strength around pylon surface is remarkably reduced by the design. The aerodynamic interference between the various parts of the optimized configuration is reduced.

References

1. Rubbert PE, Tinoco EN. Impact of computational methods on aircraft design. AIAA-1983-2060; 1983.
2. Tinoco EN, Ball DN, Rice FA. PAN AIR analysis of a transport high-lift configuration. *J Aircr* 1987;**24**(3):1812–71.
3. Chen AW, Tinoco EN. PAN AIR applications to aero-propulsion integration. AIAA-1983-1368; 1983.
4. Saitoh T, Kim HJ, Takenaka K. Multi-point design of wing-body-pylon configuration. AIAA-2006-3461; 2006.
5. Gisin YM, Marshall DD. Wing–nacelle assembly multidisciplinary performance optimization. AIAA-2007-1463; 2007.
6. Koc S, Kim HJ, Nakahashi K. Aerodynamic design of wing-body-nacelle-pylon configuration. AIAA-2005-4856; 2005.
7. Jie L, Feng WL. Numerical simulation of transonic flow over wing-mounted twin-engine transport aircraft. *J Aircr* 2000;**37**(3):469–78.
8. Rossow CC, Godard JL, Hoheisel H. Investigations of propulsion integration interference effects on a transport aircraft configuration. AIAA-1992-3097; 1992.
9. Oliveira GL, Trapp LG, Puppin-Macedo A. Integration methodology for regional jet aircraft with underwing engines. AIAA-2003-934; 2003.
10. Andreoli M, Janka A, Desideri JA. Free-form-deformation parameterization for multilevel 3D shape optimization in aerodynamics. INRIA Research Report 5019; 2003.
11. Sederberg TW, Parry SR. Freeform deformation of solid geometric models. *Comput Graphics* 1986;**22**(4):151–60.
12. Devroye L, Mucke E, Zhu B. A note on point location of Delaunay triangulation of random points. *Algorithmica* 1998;**22**(4):477–82.
13. Wang X. Study on an algorithm for fast constructing Delaunay triangulation and 3D visualization in openGL environment. *Sci Technol Eng* 2000;**9**(11):2070–4 [Chinese].
14. Chew LP. Constrained Delaunay triangulations. *Algorithmica* 1989;**4**(1–4):97–108.
15. Liu XQ, Li Q, Qin N. A new dynamic grid algorithm and its application. *Acta Aeronaut Astronaut Sin* 2008;**29**(4):817–21 [Chinese].
16. Liu XQ, Qin N, Xia H. Fast dynamic grid deformation based on Delaunay graph mapping. *J Comput Phys* 2006;**211**(2):405–23.
17. Zhu XX. *Free curve and surface modeling techniques.* Beijing: Science Press; 2000 [Chinese].

18. Leatham M, Stokes S, Shaw JA, Cooper J, Appa J, Blaylock TA. Automatic mesh generation for rapid-response Navier-Stokes calculations. AIAA-2000-2247; 2000.

19. Baker TJ. Unstructured meshes and surface fidelity for complex shapes. In: *Proc. 10th AIAA Comp. Fluid Dynamics Conf*; 1991. p. 714–25.

20. Mavriplis DJ. Unstructured grid techniques. *Annu Rev Fluid Mech* 1997;**29**(1):473–514.

21. Pepper DW, Heinrich JC. The finite element method: basic concepts and applications. *Hemisphere Publishing Corporation* 1992.

22. Jeong S, Murayama M, Yamamoto K. Efficient optimization design method using Kriging model. *J Aircr* 2005;**42**(2): 413–20.

23. Su W. Aerodynamic optimization design based on computational fluid dynamics and surrogate model [dissertation]. Xi'an: Northwestern Polytechnical University; 2007.

24. Shen Q, Yu XQ, Zhan L. Integrated optimization for wing shape and nacelle locations of transports. *Adv Aeronaut Sci Eng* 2010;**1**(1):30–5 [Chinese].

25. Jenkinson LR, Simpkin PR, Rhodes D, Jenkison LR, Royce R. *Civil jet aircraft design*. London; 1999.

Li Jing is a Ph.D. student at School of Aeronautics, Northwestern Polytechnical University. Her main research interest is aircraft design.

Gao Zhenghong is a professor and Ph.D. supervisor at School of Aeronautics, Northwestern Polytechnical University. Her current research interests are aircraft design and fluid mechanics.

Huang Jiangtao is a postdoctoral student at School of Aeronautics, Northwestern Polytechnical University. He received his Ph.D. degree from the same university in 2012. His main research interests are aircraft design and aeroelasticity.